Friction https://mc03.manuscriptcentral.com/friction
https://doi.org/10.26599/FRICT.2026.9441304

Research Article

Loose interfacial water molecule induced low friction on ice

Yuan Liu, Chang Dong, Linyuan Guo, Xinchun Chen, Liran Ma✉

State Key Laboratory of Tribology in Advanced Equipment, Department of Mechanical Engineering, Tsinghua University, Beijing 100084, China

✉ Corresponding author. E-mail: maliran@tsinghua.edu.cn

Received: November 8, 2026; Revised: August 13, 2026; Accepted: August 23, 2026

Abstract: Reducing the ice surface friction coefficient is crucial for improving the performance of winter sports equipment and enhancing the energy efficiency of icebreakers. The existence of a lubricating layer on the ice surface is the fundamental reason for the slippery ice surface. However, understanding the role of lubricating layer in ice friction presents challenges due to the complex interactions between water molecules and various materials. This study investigates the underlying mechanisms that govern ice-surface friction through advanced material design, utilizing a multiscale characterization approach that incorporates Rheometry, Raman spectroscopy, X-ray photoelectron spectroscopy (XPS) and sum frequency generation (SFG) spectroscopy. We examined the effects of interfacial lubricating layer on friction across varying sliding velocities, contact pressures, and

temperatures. Our findings indicate that three types distinct elements doped diamond-like carbon (DLC) films can achieve ultralow friction on ice, with a-C:H, a-C:H:Si, and a-C:H:WC showing reductions in the friction coefficient of 21.5%, 38.7%, and 58.6%, respectively, when compared to bearing steel (SUJ2). Here, we reveal the mechanism underlying the low friction of DLC on both ice surfaces and in water. In addition to the conventional graphitization induced low friction mechanism, the low friction coefficient is also closely associated with the presence of loosely structured interfacial water molecules, which exhibit a "liquid-like" arrangement and a disordered hydrogen bonding network that collectively contribute to the reduced friction. Additionally, molecular dynamics simulations directly visualize the contribution of loosely structured interfacial water molecules to low interfacial shear. This work presents a novel low friction material of DLC for ice surfaces. The groundbreaking discovery offers an innovative solution for friction reduction engineering in aqueous environments and for advancing competitive winter sports technology. Achieving friction reduction by regulating the molecular structure of interfacial water would be significant for the lubrication industry.

Keywords: Ice; DLC film; water molecules structure; low friction

1 Introduction

The significance of ice friction spans several research domains, such as competitive winter sports, safety in winter transportation, polar engineering, national defense, and glaciology[1-3]. In arctic shipping routes, icebreaking vessels consume up to 70% of their total power output to overcome ice friction[4, 5], highlighting the critical need for low-friction materials to reduce maintenance and operational costs. In winter sports, the friction between athletic equipment and ice surfaces plays a crucial role in determining athletes' performance outcomes. During speed skating the contribution of ice friction to the overall frictional loss is about 20%[6]. Researchers are actively working on innovative solutions to reduce ice friction for various industrial and athletic applications.

Around 7000 B.C, the earliest known instance of ice gliding was documented in Scandinavian. By 2400 B.C, sleds had been employed for transporting heavy loads, including the transport of Egyptian statues. This involved using water to lubricate the sliding surfaces[6]. And ice lubrication used for moving heavy stones to the Forbidden City in 15th- and 16th-century in China[7]. In 1859, Faraday[8] pressed two pieces of ice together and observed their refreezing, proposing for the first time that the surface of ice was covered by a layer similar liquid, which marked the beginning of research on ice lubrication. The friction coefficient on ice is notably low, primarily because of the lubricating effect of the surface water layer. Nonetheless, the mechanism behind the formation of this layer has been a topic of debate for nearly a century. Thomson proposed the pressure melting theory, suggesting that pressure decreases the melting point of ice. Previous studies had pointed out that even under high contact pressure, the effect on the melting temperature was limited. Therefore, the pressure melting mechanism alone was insufficient to explain ice lubrication[6]. Bowden and Hughes proposed the friction melting theory in 1939, suggesting that frictional heat generated during motion melts the ice surface, producing a thin water layer that acts as a lubricant[9]. Yet this also could not explain phenomena such as penguins slipping while standing motionless on ice[10]. Each of these mechanisms has specific limitations. It was not until 1949 that Gurney proposed the premelting theory, also known as the quasi liquid layer(QLL) theory[11]. Scientists have confirmed through simulations[12, 13], adsorption experiments[14], nuclear magnetic resonance (NMR)[15], micro-fluorescence spectroscopic technique[16] and other techniques that an intrinsic quasi liquid layer exists on the ice surface above -35° C, with a thickness varying from 150 nm to less than 1 nm[2, 6, 8, 17-19]. In 2024, Hong et al. discovered that the ice surface starts to melt at a temperature of -153℃[20]. Canale developed a tuning fork method capable of simultaneously probing the thickness, viscoelasticity, and friction of the water film on ice surfaces[2]. The results indicated that when an object glides over a lubricating layer on ice, this layer displays both viscous and elastic properties. As a result, it is more challenging to expel the lubricant from the gaps than it would be with regular water. The friction

experienced during this process leads to wear, which generates debris that melts into the lubricating water film. This phenomenon supports the self-lubrication theory of ice[21]. The lubricating water film exhibited properties similar to bulk water at the air interface, while it resembled ice closer to the solid ice phase. Between these two regions lies an intermediate zone characterized by a blend of ice particles and water. These findings bolster the premelting theory, which has gained broad acceptance among scholars as the primary explanation for the low friction coefficient observed on ice surfaces.

However, differing viewpoints also exist. Tusima[22] does not support the existence of a premelted layer on ice and argues that the adhesion theory can explain the low friction of ice, considering the frictional melting theory to be logically contradictory. Weber[23] and Liefferink[24] suggest that the high mobility of surface molecules is key to ice lubrication. Demmenie[25] found that sublimation from and condensation onto the ice surface was the dominant scratch-healing mechanism, at odds with surface diffusion or fluid flow or evaporation-condensation from a quasi liquid layer. Their works on icicle surface ripples[26] and partial wetting[27] confirm water did not wet ice, inconsistent with a layer of water on the surface of ice. Nagata et al[28] discussing SFG shown the surface was disordered but not liquid under equilibrium. These scholars' perspectives offer different insights into the understanding of ice friction mechanisms. Nevertheless, while the exact nature of the interfacial layer remains a subject of discussion, the low friction on ice is widely attributed to the weak interaction and high mobility of interfacial water molecules.

The premelted layer on ice generally measures less than 150 nm in thickness. However, because the surface roughness of ice can vary from hundreds of nanometers to several micrometers, this thin water film is inadequate to entirely cover the ice surface's asperities. Based on the relationship of film thickness ratio and friction coefficient[29], the lubrication state at this stage might be classified as boundary lubrication. However, factors such as temperature and applied pressure on the ice surface can further increase the actual thickness of the water film[6], with the water film thickening, the lubrication state maybe enter mixed lubrication or even hydrodynamic lubrication. The coefficient of

friction (COF) on ice depends on the interplay between the sliding sample, the ice substrate, and the liquid-like layer at their interface. These three factors collectively determine the frictional behavior[30]. The COF on ice can be reduced not only by adjusting experimental conditions such as temperature[10, 24], sliding speed[3, 31-33], normal load[21, 24, 32], and ambient humidity[6], but also by optimizing material properties, wettability[2, 34], surface roughness[24] and thermal conductivity[35]. Additionally, the COF depends on the properties of the ice itself. For instance, when ice containing salt ions, the concentration and composition of these ions can significantly affect ice friction[33, 36, 37]. The presence of salt ions is known to decrease the friction coefficient of ice. Consequently, when the geometry of the friction pair, testing conditions, and ice composition remain constant, altering the material properties of the counterface that slides against the ice emerges as the most effective approach to minimize ice friction. Despite more than a century of research into the principles governing ice friction, substantial controversies continue to exist concerning the mechanisms at play, which has impeded the advancement of effective methods for reducing ice friction. Therefore, it is crucial to uncover the fundamental mechanisms involved and to create innovative materials aimed at lowering the coefficient of ice friction.

The natural occurrence of a premelted layer or high mobility water molecular on the surface of ice indicates that ice friction fundamentally relies on the role of water molecular to facilitate lubrication. With the progress of water lubrication technologies, researchers have delved deeply into the mechanisms through which interfacial water molecular minimizes friction. The Stribeck curve facilitates the classification of lubrication regimes into three primary zones: boundary lubrication, mixed lubrication, and hydrodynamic lubrication[38]. Key friction-reducing mechanisms include: electrical double-layer effects[39], hydration effects[40], hydrodynamic pressure effects[41]. Probing the structure of water molecules at the solid-liquid interface and understanding their impact on friction are significant challenges. Monitoring water molecules at the solid-water interface is essential for

understanding friction, yet the lack of a more detailed microscopic view of friction-reduction mechanisms has constrained the development of lubrication systems.

This study introduces an effective method for reducing friction in icy conditions by applying diamond-like carbon (DLC) films (a-C:H, a-C:H:Si, and a-C:H:WC) to steel substrates. The Verein Deutscher Ingenieure classifies DLC into seven categories based on its elemental composition and structural characteristics[42]. The DLC films studied in this work are hydrogenated amorphous carbon films, specifically including hydrogenated amorphous carbon (a-C:H), metal-doped hydrogenated amorphous carbon (a-C:H:WC), and modified hydrogenated amorphous carbon (a-C:H:Si). We validated the feasibility of this approach by examining its performance under varying speeds, loads, and temperatures. Our findings indicate that the reduction in friction observed with DLC films is primarily due to the presence of a "liquid-like" structured water molecular layer at the interface, a conclusion supported by the innovative use of sum frequency generation (SFG) spectroscopy. This revelation suggests that materials with a dominant "liquid-like" interfacial water structure can effectively tackle high friction issues encountered in icy conditions, lower energy consumption in ice breaking vessels, and improve performance in winter Olympic speed sports. The mechanism we elucidated allows for control of friction in icy environments. By engineering materials to enhance this "liquid-like" interfacial water layer, we could transform tribological performance in water-related applications.

2 Materials and methods

2.1 Experimental materials

The upper friction pair utilized in the ice friction experiment consisted of a ball with a diameter of 12.7 mm. The bearing steel (SUJ2) ball was purchased from Chunzhongdao Machinery (Taicang) Co. LTD, while the silicon nitride ball was purchased from New DELong Special Ceramics (Dalian) Co. LTD, and the silicon dioxide(SiO_2) ball titanium dioxide (TiO_2) ball and DLC-coated balls were created by depositing SiO_2, TiO_2 and DCL films onto the surface of the SUJ2 ball. The ice surface elastic modulus

and Poisson's ratio of were 0.75 GPa and 0.33, respectively[24]. The details of the upper friction samples were presented in Table 1[1, 43, 44]. The contact pressure between different materials and the ice surface were calculated using the Hertzian contact pressure formula[45], which was critical for interpreting results and comparing with literature. The elastic modulus of the three DLC materials were measured using Nanometer Scratch Tester. To ensure cleanliness, the experimental balls underwent ultrasonic cleaning with acetone and anhydrous ethanol for 5 min each. Following this, they were rinsed twice and subjected to ultrasonic cleaning with ultrapure water for another 5 min. The samples were then dried in a drying oven at 40℃ for 2h. The lower friction pair consisting of ice, was prepared by freezing ultrapure water in a refrigerator set to -20℃ for 2 h. The ultrapure water was purified using a water purification system from (Thermo Fisher Scientific), achieving a resistivity of of 1.43 MΩ cm.

Table 1 The contact pressure between the friction pair and the ice in the experiment.

Material	Elastic modulus (GPa)	Poisson's ratio	Hertz contact pressure (MPa)
SUJ2	208	0.25	19.47
Silicon nitride (Si_3N_4)	310	0.26	19.49
Silicon dioxide (SiO_2)	55.6	0.16	19.33
Titanium dioxide (TiO_2)	284.5	0.36	19.49
a-:C:H:Si	193	0.3	19.47
a-:C:H	167	0.3	19.46
a-:C:H:WC	163	0.3	19.46

2.2. Characterization of material surface

Surface hardness measurements were performed using a commercial Nanometer Scratch Tester (CSM Instruments). The testing involved a linear loading phase, where the load increased at a rate of 20 mN/min until a peak load of 10 mN was reached. This was followed by 2 seconds holding period at the maximum load. The surface roughness of spherical materials utilized in ice friction experiments

was assessed using a three-dimensional white-light interferometric surface profiler(ZYGO NexView). The measurement covered an area of 834.37 × 834.37 μm². The roughness of the ice surface was tested using a three-dimensional white light interferometric surface profiler. Before and after the friction experiment, the ice blocks were moved from the -20°C refrigerator to the topography testing room. To avoid the ice melting at room temperature, a low-temperature control plate was added to the testing platform of the topography tester. The contact angle (CA) was measured using an optical goniometer (DataPhysics OCA25) with 2 μL ultrapure water droplets. Raman spectral analysis (Horiba LabRAM HR800) was conducted on DLC films to track sp^2/sp^3 bond transformation induced by sliding friction. The wavelength of the Raman light source was 514 nm. Additionally, X-ray photoelectron spectroscopy (XPS, PHI Quantera II) was performed to examine changes in binding energy before and after friction at the contact area.

2.3 Ice surface friction test

The friction coefficient between the spherical sample and the ice surface was measured using the low-temperature three-ball-on-plate module of a rotational rheometer (Anton Paar MCR301). The MCR301 rheometer can achieve temperatures as low as -150°C, with cooling provided by liquid nitrogen in a sealed cavity. Due to the liquid nitrogen cooling method, the test chamber remained relatively sealed. The continuous flow of low temperature dry nitrogen gas, generated by the vaporization of liquid nitrogen, purged the contact interface, effectively eliminating the interference of ambient moisture and ensuring that the experiments were conducted under low-humidity conditions. The upper friction pair consisted of a ball with a diameter of 12.7 mm. The lower friction pair comprised three ice blocks placed equidistantly at a 45° angle to the normal direction. Ultrapure water was poured into a mold, and the mold was placed in a freezer at -20°C for 2 hours. The mold was filled with ice, forming ice blocks with dimensions of 12.9 mm × 3.9 mm × 3 mm, which were then fixed to the low-temperature rheometer using bolts. A schematic diagram of the sample installation was shown in Fig. 1(a). The 12.7 mm ball was clamped into a connector, and the connector was mounted onto the

rheometer. After the experiment began, the sensor recorded the torque to calculate the friction force, and the friction coefficient was obtained by dividing the friction force by the normal load. The experimental conditions in this study included a normal load range of 1–21 N, a rotational speed range of 1–3300 rpm (corresponding to a linear velocity range of 0.00047–1.55 m/s), and a temperature range of –40°C to –1.5°C. Extensive repeated experiments were conducted under various speeds, loads, and temperatures, and results with good reproducibility are reported. Most experiments were conducted under a load of 9 N. Based on the three-ball-on-plate module of the rheometer, the contact load perpendicular to one of three ice surface was 2.12 N. Since the elastic modulus of ice was 0.75 GPa, which was significantly lower than that of the other materials, the contact pressures during friction between different materials and the ice surface exhibit negligible differences at same load, as shown in Table1. Prior to tribological testing, the sample surfaces were characterized using optical microscopy (Keyence VHX6000), three-dimensional white light interferometric surface profiler, XPS, and Raman spectroscopy. Following rheometer testing, the wear tracks were analyzed using the same surface characterization methods to assess the chemical and topographical changes induced by tribological interactions.

2.4 Microscopic underwater friction test

Microscopic friction characterization of five materials were conducted using Atomic Force Microscope (AFM, Bruker ICON) in aqueous environment. For these measurements, 23 μm diameter silica microspheres were affixed to tipless rectangular cantilevers (TL-CONT) using epoxy adhesive followed by complete curing. The fabricated SiO_2 probes (Fig. S1) were cleaned by plasma treatment (Harrick Plasma PDC-32G) for 2 minutes prior to testing. The normal spring constant and lateral sensitivity of the AFM probes were calibrated using the thermal tune method and the improved wedge method[46]. The friction experiments were conducted in the lateral force mode (LFM) under ultrapure water environment in room temperature was shown in Fig. S2. To ensure the accuracy of the

experiment, conducted three parallel experiments and take the average value. Friction test scanning area was set to $1\times1\mu m^2$ with the scan velocity of 2 μm/s.

2.5 Characterization of interface water molecular structure

To clarify the effect of interfacial water molecular behavior on friction mechanisms for SUJ2, silicon nitride (Si_3N_4), and DLC materials, the structure of water molecules adsorbed on material surfaces was characterized using SFG spectroscopy[47], with detailed instrumentation described in the Supporting Information and Fig. S3. In the SFG experiments, the spatial and temporal overlap of visible (Vis) and infrared (IR) beams was established at the sample measurement position, employing incident angles of 45° (Vis, 30 mW) and 60° (IR, 16 mW) in a PPP polarization configuration, with sample sizes maintained between 1-3 cm. The test samples included polished SUJ2, Si_3N_4, and coatings of a-C:H:Si, a-C:H, and a-C:H:WC films. Before testing, each sample was positioned at a 45° tilt and rinsed with 20 mL of ultrapure water. The water was poured onto the top of the sample , allowing it to flow down the surface, with the effluent collected in a beaker. The adsorption capacity and structural arrangement of water molecules exhibited considerable variation across different material surfaces. At each measurement point, five infrared center wavelengths were applied sequentially (2900 nm, 3000 nm, 3100 nm, 3200 nm, and 3300 nm). The true SFG signal was obtained by summing the signals of each wavelength and subtracting the background signal at each corresponding wavelength.

2.6 MD simulation

Two different models were built to investigate the different materials sliding. The first model (a hydrogenated amorphous carbon (a-C:H)/ice system) consisted of a a-C:H slab at the top and an ice slab at the bottom. The second model (steel (Fe)/ice system) included a Fe silica slab at the top and an ice slab at the bottom. The amorphous carbon (a-C:H) slab with a C:H molar ratio of 80:20 was generated via a melt-quench protocol using the ReaxFF reactive force field[48]. The preparation involved melting at 4500 K, three annealing cycles between 3000 K and 1000 K, and finally cooling to 300 K. The Fe slab was created by cleaving a bulk bcc-Fe crystal along the (001) plane. Both solid

slabs were approximately 30 Å thick, with lateral dimensions of L_x = 109.5 Å and L_y = 40.6 Å to match the underlying ice slab. The ice slab, identical in both models, consisted of 9072 water molecules initially arranged in the hexagonal ice (Ih) phase, with a total thickness of approximately 66 Å (9072 molecules). In the final model (Fig. 6(a) and (b), the 30 Å of solid slabs served as the top sliders, while the lowermost 26 Å of the ice layer was fixed to act as a rigid substrate (ice substrate). A vacuum region of approximately 50 Å was introduced above the top slider to ensure free surface conditions. Periodic boundary conditions were applied in the x and y directions, while non-periodic boundary conditions were used in the z direction. For the sliding simulations, the atomic interactions within the solid slabs (a-C:H and Fe) were described using the Consistent Valence Force Field (CVFF)[49]. The water molecules were represented by the rigid five-site TIP5P-E model[50], which explicitly includes lone-pair sites to accurately reproduce the water phase diagram. Cross-interactions between different atomic species were determined using arithmetic mixing rules. Additionally, we acknowledge that the choice of water model can significantly influence the behavior of interfacial water. The TIP5P-E water model has been widely validated for ice-water interfacial systems. Previous studies have demonstrated its reliability in describing key properties such as the melting point of ice Ih[51] and ice melting behavior[52]. TIP5P-E accurately reproduces the structural and dynamic properties of water near solid surfaces, making it a suitable choice for the present investigation.

All molecular dynamics simulations were performed using the LAMMPS package[53]. During the sliding phase, the top slider was treated as a rigid body. A normal load of 14.5 MPa was applied to the rigid slider, which was driven at a constant velocity of 50 m/s in the x-direction. The mobile water molecules (the uppermost 40 Å of the ice slab) were coupled to a Nosé-Hoover thermostat[54] at 266.15 K with a relaxation time of 100 fs. The TIP5P-E model was selected for its ability to accurately reproduce the melting temperature (approx. 271 K[51]) and tetrahedral structure of ice Ih. The simulation temperature of 266.15 K corresponds to an undercooling of ~5 K, ensuring the stability of the ice phase while allowing for interfacial premelting. The simulation box dimensions were chosen

to be commensurate with the lattice constants of Ice Ih, resulting in a lattice mismatch of less than 0.3% in both x and y directions, thereby minimizing strain in the ice slab. The equations of motion were integrated using the velocity-Verlet algorithm with a time step of 1.0 fs. Short-range van der Waals interactions were calculated with a cutoff distance of 12 Å, while long-range electrostatic interactions were computed using the Particle-Particle Particle-Mesh (PPPM)[55] method with a relative precision of 10^{-5}. The total simulation time was 10.0 ns, and data from the final 5.0 ns were collected for steady-state analysis.

3 Results and Discussion

3.1 Experimental results of ice surface friction

The schematic diagram of the ice friction system is depicted in Fig. 1(a). Fig. 1(b) illustrates how the ice friction coefficient varies with sliding velocity for various materials, tested under a normal load of 9 N at -7 °C. The sliding speed was incrementally increased from 0.00047 m/s to 1.55 m/s over the initial 180 s of friction, followed by a steady state sliding period at 1.55 m/s for the subsequent 300 s. The materials used in the experiments included SUJ2, Si_3N_4, SiO_2, TiO_2 and three types of DLC materials: hydrogenated amorphous carbon film (a-C:H), modified hydrogenated amorphous carbon film (a-C:H:Si), and metal-compound-doped hydrogenated amorphous carbon film (a-C:H:WC). The experimental findings revealed that during the initial linear increase in sliding velocity, the friction coefficient for all materials on ice rapidly increased before subsequently decreasing. Once the velocity stabilized at 1.55 m/s, the friction coefficient also reached a steady state, exhibiting only minor fluctuations with a gradual increase toward the conclusion of the measurement period. The friction coefficient of SUJ2 steel on ice falls within the range reported in the literature[1, 24, 33]. Based on the statistical results of at least three experiments, the mean friction coefficients and error bars for different materials on ice under the conditions of 1.55 m/s, 9 N, and -7°C were presented in Fig. 1(c). According to the surface premelting theory, a nanoscale quasi-liquid water film naturally exists on the surface of the ice. At the initial low velocity stage, the rise in the friction coefficient can be attributed to the

lubricating water film's thickness being significantly less than the height of the surface asperities. As a result, the upper friction counterpart primarily interacted with the ice through contact at the asperities. During sliding, the ice asperities experienced fracture, sintering, and stick-slip phenomena at these extremely low speeds, which contributed to the increase in friction[32, 33, 56-58]. The friction melting theory posits that the heat generated from sliding movements elevates the temperature at the points of contact between asperities. As velocity increases, it produces greater frictional heat, which accelerated the melting of localized ice and leads to the formation of a lubricating water film. However, the lubricant film thickness remained smaller than the composite surface roughness, indicating that the friction was in the boundary lubrication regime, which led to a decrease in the friction coefficient with increasing sliding velocity. The critical velocity at which the friction coefficient shifts from an increase to a decrease varies based on the material properties involved. Furthermore, the pressure melting theory suggests that the application of pressure enhances the melting of ice even further[21]. The particles produced from ice fracture and abrasion melt upon absorbing heat, leading to the formation of a lubricating water film. With progressive film thickening and improved continuity, both the water film and surface asperities work together to support the load, maight indicating a shift to mixed lubrication. As the water film grows further, the system ultimately enters the hydrodynamic lubrication regime. In this state, the thickened film resists motion, leading to a slight increase in friction. This velocity dependent behavior aligns well with the model proposed by Schulson[56]. The experiments were conducted under low humidity conditions. Therefore, this further indicated that the lubricating water film originated from the friction system itself, and the influence of external humidity was precluded. After the friction coefficient stabilized, the three DLC materials demonstrated significantly better ice friction reduction performance compared to SUJ2, Si_3N_4, SiO_2 and TiO_2. Under sliding speed at 1.55 m/s, the DLC films achieved ice friction reduction rates of 21.5% (a-C:H:Si), 38.7% (a-C:H), and 58.6% (a-C:H:WC) relative to SUJ2, as shown in Fig. 1(d).

The load experienced by low temperature equipment fluctuates under various working conditions. For example, when athletes glide on ice, changes in their posture affect the contact area between their skate blades and the ice, resulting in variations in contact load. Consequently, it is crucial to examine how load influences ice-surface friction. In the experiment designed to explore the relationship between load variation and the ice surface friction coefficient, the sliding velocity was maintained at a constant 1.55 m/s, and the temperature was set at -7℃. The load was systematically varied from 1 N to 21 N, with each test conducted over a duration of 300 s. During the trials with increasing load, the friction coefficient exhibited a decline before ultimately stabilizing. Notably, the DLC films consistently demonstrated a lower friction coefficient on the ice surface compared to both SUJ2 and Si_3N_4 throughout the testing, as illustrated in Fig. 1(e).

An increased in load shifted the Stribeck curve to the left[38], essentially reducing the lubrication film thickness by squeezing. However, the most distinctive characteristic of ice, compared to other solid surfaces, was its ability to continuously generate a lubricating water film during the friction process. In addition to frictional heating, which produces meltwater, an increase in load induces the transformation of ice's crystalline structure into liquid water under pressure, further contributing to water film formation, a finding consistent with the work of Baran[46]. Moreover, ice wear particles generated during sliding could melt under frictional squeezing and compression, also contributing to the thickening of the water film. While an increase in pressure tends to squeeze the water film out of the contact zone, frictional action simultaneously promotes film thickening, resulting in a dynamic competition and balance between these two effects[59-61]. A key characteristic of ice, however, is that even when water is squeezed out of the contact area, fresh ice can continuously melt to supply lubricating water to the contact zone. Therefore, under the conditions investigated in this study, an increase in contact pressure leads to a reduction in the friction coefficient. Nevertheless, this trend is not universal, some studies have reported that for certain materials, ice friction increases or remains largely unchanged with increasing pressure [6, 24]. The effect of pressure on the friction coefficient

was closely related to the material properties, lubrication regime, and experimental conditions. For instance, in the work of Liefferink[6], when the speed was below 0.1 m/s, the system operated in the boundary lubrication regime, where an increase in pressure led to a rise in the friction coefficient.

In our experiment exploring the relationship between temperature variation and the friction coefficient on an ice surface, the sliding velocity was maintained constant at 1.55 m/s under a fixed load of 9 N. The temperature was systematically varied from -40°C to -4°C, with each test lasting 300 s. The influence of temperature on the friction coefficient is presented Fig. 1(f). We observed that the friction coefficient for all materials decreased as the temperature increased. Notably, SUJ2 and Si_3N_4 exhibited higher friction coefficients compared to DLC films. Fig. S4 demonstrated the friction behaviour near-freezing-point, indicating that the friction coefficient of SUJ2 first decreased and then increased within the -7°C to -1.5°C range. The reduction in the friction coefficient with increasing temperature can be attributed to the thickening of the lubricating water film. However, the observed increase near 0°C may stem from two competing mechanisms: first, as the temperature approaches the melting point, the water film thickness reaches a critical level that causes the lubrication regime to transition from mixed to hydrodynamic lubrication. In this state, an excessively thick water film may hinder sliding. Second, the softening of ice at higher temperatures allows the counterface to penetrate more deeply into the ice surface, resulting in increased plowing resistance. This was consistent with the research conclusion of the Tusima and Bonn group[22, 23]. Both factors likely contribute to the observed rise in friction near the melting point.

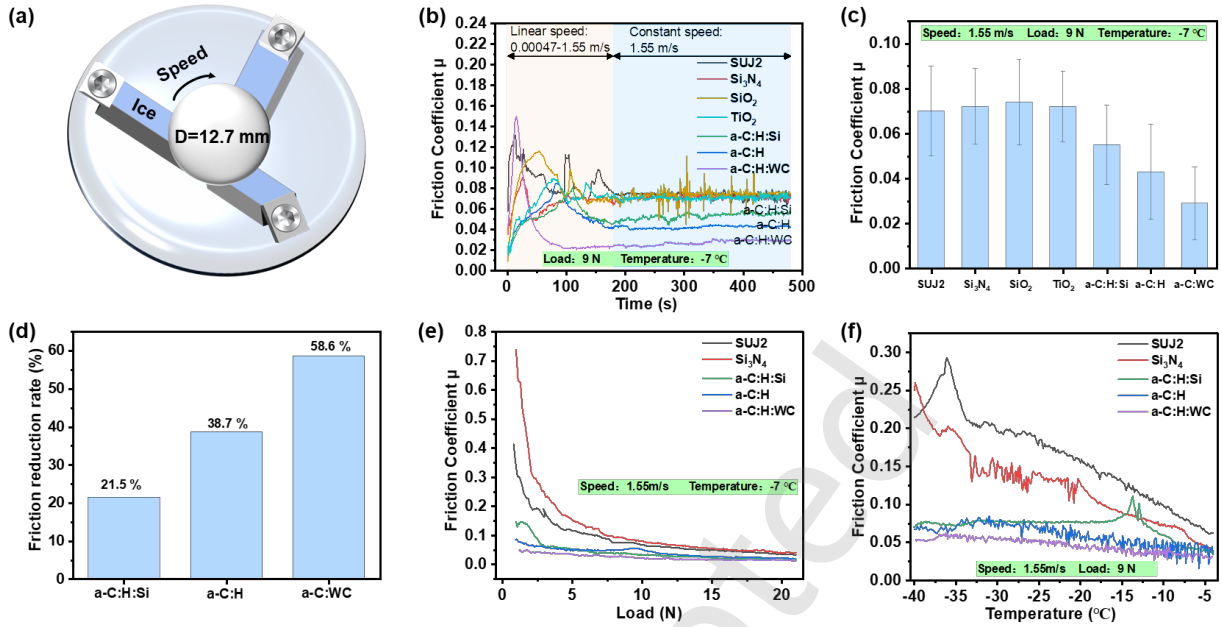

Fig. 1 Characteristics of ice friction. (a) Schematic of the ice surface friction system; (b) Variation curve of the ice surface friction coefficient with sliding velocity; (c) Mean friction coefficients of different materials on ice at a speed of 1.55 m/s, a load of 9 N, and a temperature of -7°C; (d) Friction reduction rate of DLC material compared to SUJ2 on ice; (e) Variation curve of the ice surface friction coefficient with applied load; (f) Variation curve of the ice surface friction coefficient with temperature.

3.2 The form of wear caused by ice surface friction

Friction surface, the occurrence of wear, and the wear forms were used for evaluating the tribological properties of materials. In this study, wear analysis was conducted on materials in contact with ice surfaces. Before the experiments, optical microscopy was used to capture images of the original surfaces, as shown in Fig. 2(a)-(e). The wear tests were then carried out at a sliding speed of 1.55 m/s, a load of 9 N, and a temperature of -7°C. After 10 minutes of friction, optical images of the contact area were obtained, as shown in Fig. 2(f)-(j), along with three-dimensional topographical representations of the worn surfaces displayed in Fig. 2(k)-(o).

Initially, the a-C:H:WC film presented a relatively rough surface, characterized by protrusions and pits, as seen in Fig. 2(e). In contrast, the surfaces of the other materials appeared smooth, exhibiting no visible signs of wear or damage. Post-experiment, the SUJ2 surface displayed pronounced scratches,

indicative of typical abrasive wear, predominantly caused by the ploughing effect, with nearly the entire area marked by these scratches. Fig. S5 presents the three-dimensional topography of the ice surface before and after sliding against the SUJ2. The ice surface was flat before friction, and pronounced grooves were seen after friction, matching the shape of the wear marks on the surface of SUJ2. During sliding, asperities of SUJ2 surface ploughed through the ice, inducing plastic flow and forming grooves. Simultaneously, ice surface asperities also contributed to the wear of the SUJ2 generating ploughing scratches.

This study demonstrated that not only do harder materials wear down softer ones, but even relatively soft materials like ice can cause wear on harder substrates. Both optical images and three-dimensional white-light topography confirmed minimal wear on the Si_3N_4 surface. The hardness measurements summarized in Table 2 indicate that Si3N4 demonstrated the highest hardness, consistent with its superior wear resistance. The a-C:H:Si film surface exhibited characteristic scratches, indicative of abrasive wear stemming from a ploughing mechanism, as shown in Fig. 2(m). The a-C:H film exhibited both ploughing scratches and a localized peeling pit, marked by the solid-line circle in Fig. 2(i). The a-C:H film thickness of approximately 1.3 μm and a peeling depth of about 0.38 μm (Fig. S6), the observed damage was consistent with fatigue-induced crack propagation in near-surface regions. This peeling is attributed to subsurface crack growth under cyclic loading, eventually leading to partial delamination of the coating. The hydrogen embrittlement effect in hydrogenated DLC (a-C:H) under humid and low-temperature conditions likely expedited the initiation of fatigue. Notably, the 10-minute friction test duration was sufficient to induce initial fatigue damage, particularly at the high sliding speed of 1.55 m/s.

While optical microscopy revealed minor scratches on the a-C:H surface in Fig. 2(i). The surface roughness decreased from an initial Sa value of 134 nm to 53 nm post-wear testing, indicating that the sharp asperities on the a-C:H:WC film were progressively worn down during friction, resulting in a

smoother surface with mild polishing marks. Notably, no bulk material delamination was detected, and the primary wear mechanism was classified as abrasive wear.

In summary, the wear behaviour of various materials on ice surfaces significantly correlates with material hardness. The SUJ2, having relatively lower hardness, exhibited pronounced abrasive wear characteristics. Among the three types of DLC films tested, all surfaces showed mild abrasive wear, with the a-C:H coating additionally displaying slight fatigue wear. Conversely, the Si_3N_4 surface, possessing the highest hardness, demonstrated excellent wear resistance with no detectable surface damage.

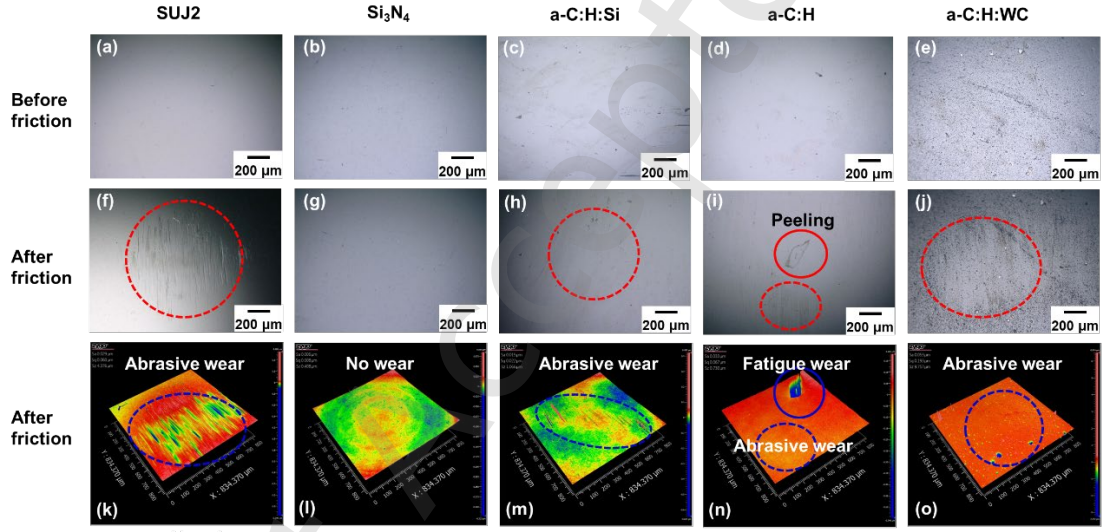

Fig. 2 Wear characteristics of materials on ice surfaces. (a-e) Optical images of SUJ2, Si_3N_4, a-C:H, a-C:H:Si, and a-C:H:WC films before friction experiment; (f-j) Corresponding optical images after friction experiment; (k-o) Three-dimensional white-light interferometry topography of wear surfaces.

It was worth noting that the wear mechanism during ice friction was significantly different from that in conventional friction. Due to frictional heating, the interfacial temperature increases, causing wear debris (ice particles) to spontaneously melt and transform into liquid water. This made traditional wear particle tracking (e.g., counting or morphological analysis) difficult to implement and of limited significance for interpreting friction behavior. This solid-liquid phase transition was precisely the core characteristic of ice self-lubrication[21]: the wear product (water) directly participated in the formation

of the lubricating water film and governed the evolution of the friction coefficient, rather than becoming embedded in the interface as solid particles.

3.3 Characterization of material surface physical properties

The characteristics of material hardness, surface roughness, wettability, and surface potential all have a direct impact on friction. To explore the friction-reducing mechanism of DLC materials on ice surfaces, these properties were thoroughly characterized, and the results were shown in Table 2. The hardness of SUJ2 obtained through nano-hardness tester was the lowest (3.99 GPa), while Si_3N_4 was the highest (32.23 GPa). The hardness values for the three types of DLC film, a-C:H:Si, a-C:H, and a-C:H:WC, were 24.32 GPa, 22.88 GPa, and 17.62 Gpa, respectively. Although the hardness of SUJ2 coated with DLC film had increased compared to the original surface, the results of the hardness combined COF indicate that high hardness did not necessarily to low ice friction coefficient. Thus, the mechanism of DLC friction reduction need to be considered other properties of the material. The surface roughness of friction pairs influenced the contact type between two surfaces, subsequently influencing the lubrication regime. In the ice friction system, the upper friction pair consisted of a 12.7 mm diameter ball. The surface roughness of the spherical material was quantified using Sa (arithmetical mean height). Notably, the a-C:H:WC film exhibited the highest roughness at Sa = 134 nm, which initially resulted in the highest friction coefficient peak under low-speed conditions (Fig. 1b). However, once steady-state friction was reached, the a-C:H:WC film demonstrated the lowest ice friction coefficient. At this steady state, the surface roughness of the a-C:H:WC film had a smaller roughness (Sa = 53 nm) compared to the original surface (Sa = 134 nm), as illustrated in Fig. 2(o). In comparison, the other four materials, SUJ2 (Sa = 4 nm), silicon nitride (Sa = 7 nm), a-C:H:Si film (Sa = 9 nm), and a-C:H film (Sa = 8 nm) were not significantly different, but the friction coefficients vary greatly. This suggested that ice friction reduction was not strongly correlated with surface roughness across different materials and indicating the presence of other mechanisms.

Surface wettability also affects the interaction between the material surface and the lubricating water film. The balance between hydrophilicity and hydrophobicity can alter the competitive adsorption of water molecules on the material surface, thereby modifying the lubrication state. Consequently, friction is intrinsically connected to the surface wetting conditions. Contact angle measurements were performed on various material surfaces, and the results are summarized in Table 2. Si_3N_4 demonstrated higher hydrophilicity than other materials, while the wettability of the remaining materials was comparable. Interestingly, the observed wettability trends did not directly relate to the ice friction coefficients of the materials in this system.

Furthermore, surface potential altered the molecular repulsion or attraction at the material interface, thereby affecting frictional properties. Surface potential measurements were conducted on all tested materials, with results presented in Table 2. Si_3N_4 and a-C:H:WC showed similar levels of negative potential. However, these two materials demonstrated significantly different friction coefficients. SUJ2 exhibited a weakly positive potential, but friction coefficient was comparable to that of silicon nitride. No clear correlation was found between variations in surface potential and ice friction coefficients across the tested materials.

Table 2 Measurement of the physical characteristic parameters of the friction pair.

Materials / Characteristic	SUJ2	Silicon Nitride	a-:C:H:Si	a-:C:H	a-:C:H:WC
Hardness (GPa)	3.99	32.23	24.32	22.88	17.62
Roughness (nm)	4	7	9	8	134
Contact Angle (°)	83	36	88	75	79
Surface Potential (mV)	3.72	-28.57	-50.99	-45.22	-20.24

3.4 Mechanism of friction-reduction on ice surfaces

3.4.1 Spectroscopic evidence of sp^2-induced lubrication in DLC-ice tribosystems

To clarify the underlying mechanisms responsible for the remarkable friction-reducing capabilities of DLC films on ice surfaces, Raman spectroscopy was conducted on the surface both prior to and following friction testing. Typically, the Raman spectrum of DLC films exhibited two characteristic peaks: the G peak (1550–1600 cm^{-1}) and the D peak (~1350 cm^{-1})[62]. The G peak reflected the ordering of sp^2 hybridized carbon in the material and was caused by the E_2g bond stretching vibration (e.g., C=C bonds in graphene, chains, or rings of sp^2 carbon)[63]. When sp^2 carbon in DLC forms nanocrystalline or disordered graphite structures, lattice defects leaded to the appearance of the D peak, which caused from the breathing mode (A_1g) of sp^2 carbon[63, 64]. The Raman spectra of a-C:H:Si, a-C:H, and a-C:H:WC films before and after friction with ice surfaces were presented in Fig. 3. The D and G peaks were obtained by Gaussian fitting of the Raman spectra. The intensity ratio of the D peak to the G peak (ID/IG) could be used to assess the ordering of sp^2 carbon: An increase in ID/IG generally indicated a higher sp^2/sp^3 ratio, suggesting a greater proportion of disordered sp^2 carbon and an increased level of graphitization in the material[65]. Following ice-surface friction, the three types of DLC materials exhibited an increased D-peak intensity ratio, indicating an increase in sp^2-bond content at the surface. This observation implies that the frictional interaction with ice induced graphitization of surface layers during sliding. DLC films possess a metastable amorphous structure that lies between diamond and graphite. During friction, the combination of high localized contact pressure, frictional heating, and shear forces promoted the breaking of C-H bonds in sp^3-hybridized areas. The removal of hydrogen further facilitated the transition from sp^3 to sp^2 hybridization[66]. Simultaneously, hydrogen trapped in lattice vacancies within the DLC was released under shear, further driving the conversion to sp^2 -hybridized graphitic structures[67]. These structural changes contributed to the reduction in the coefficient of friction between the DLC film and ice.

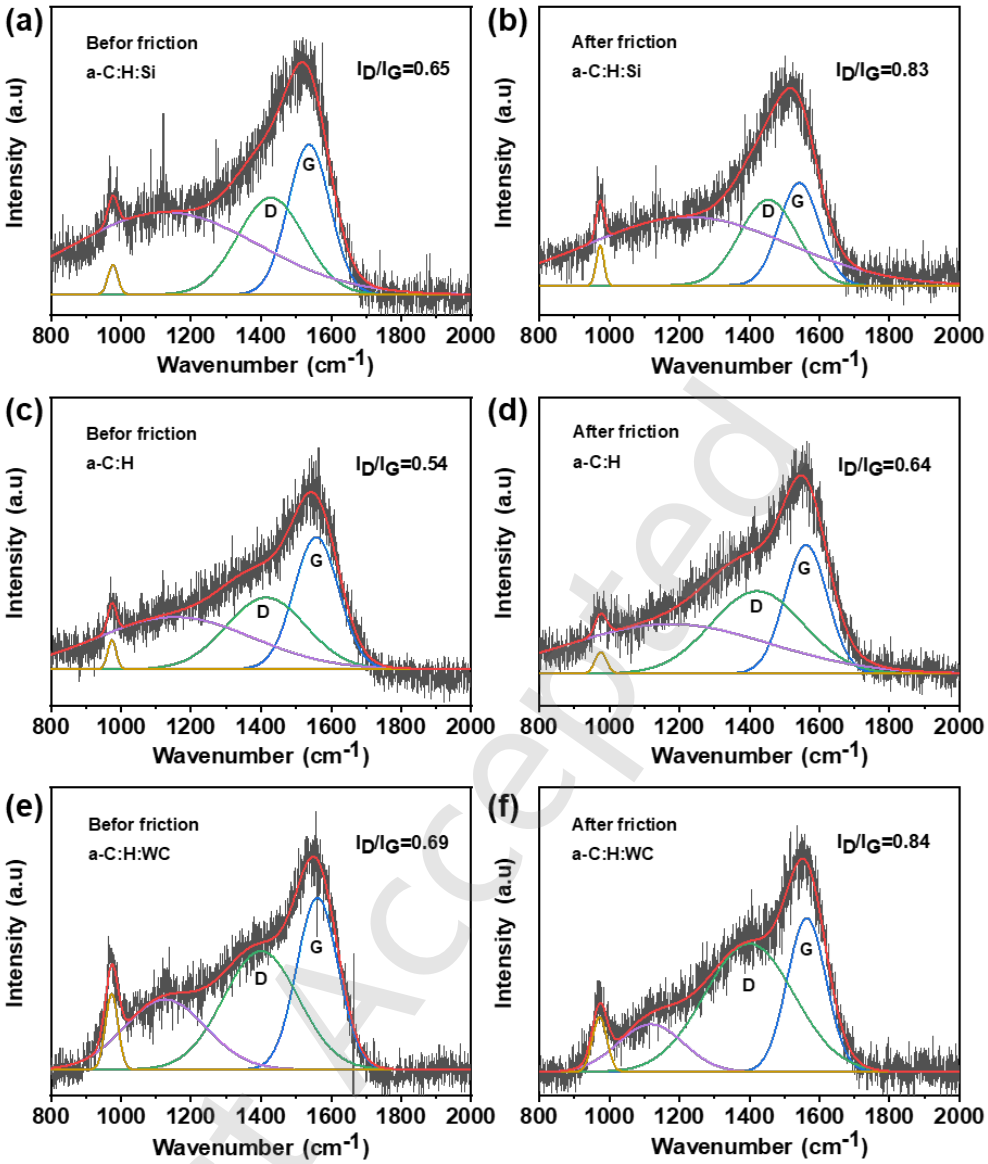

Fig. 3 Raman spectra and peak fitting curves of DLC films before and after friction. (a) a-C:H:Si original surface before friction; (b) a-C:H:Si worn track region after friction; (c) a-C:H original surface before friction; (d) a-C:H worn track region after friction; (e) a-C:H:WC original surface before friction; (f) a-C:H:WC worn track region after friction.

XPS high-resolution spectroscopy enables the detection of surface chemical bond information. Each bond exhibits a distinct binding energy, allowing for detailed analysis. In this study, peak analysis was conducted on the measured C1s spectrum, which facilitated the calculation of the relative content of sp^3 and sp^2 bonds in the DLC films by fitting the peak areas. The chemical bonds present in DLC films typically include C=C, C-C/C-H, C-O, and C=O, with C=C representing the sp^2 carbon bond and C-

C/C-H corresponding to the sp^3 C bond[68]. The XPS spectra of the DLC film before and after friction were tested, as described in Fig. 4. The peak with a binding energy of 284.0-284.5 eV belongs to the C=C bond in the thin film, 284.8-285.2 eV corresponds to the C-C bond, and the high binding band of 285.5-288.5 eV corresponds to the C-O/C=O bond. The peak areas of C=C bond and C-C/C-H can be obtained by fitting the spectra, and the peak area ratio is the ratio of sp^2/sp^3 hybrid bond. The result showed that the sp^2/sp^3 value of the surface after friction was higher than that of the original surface, which proved that the friction interface of DLC film was graphitized. The graphitized region had a very low shear strength [69], reducing the interface friction coefficient[70].

The Raman light source used for the test was 514 nm visible light. The visible light source was only sensitive to sp^2 bond and cannot excite sp^3 bond signal. Therefore, Raman could not detect sp^3 bond directly. The change trend of sp^2 and sp^3 was seen through the ratio of ID/IG. The detection depth of Raman was on the order of 100 nanometers. XPS could quantitatively calculate the sp^2/sp^3 ratio, but the detection depth was only a few nanometers, which can only analyze the surface chemical changes. The results from both XPS and Raman spectroscopy confirmed that the surface of the DLC film underwent graphitization due to friction at various spatial locations. The graphitization process reduces the friction coefficient of the ice surface, which is a traditional and typical mechanism for the low friction property of DLC materials. Graphitization occurs under the friction of certain time and pressure. Therefore, graphitization cannot take place immediately at the very beginning of the friction process. However, the DLC material exhibited excellent tribological properties at the onset of friction (as illustrated in Fig. S7). Consequently, the dominant mechanisms underlying the reduction of friction in DLC on ice need further investigation through more direct methods.

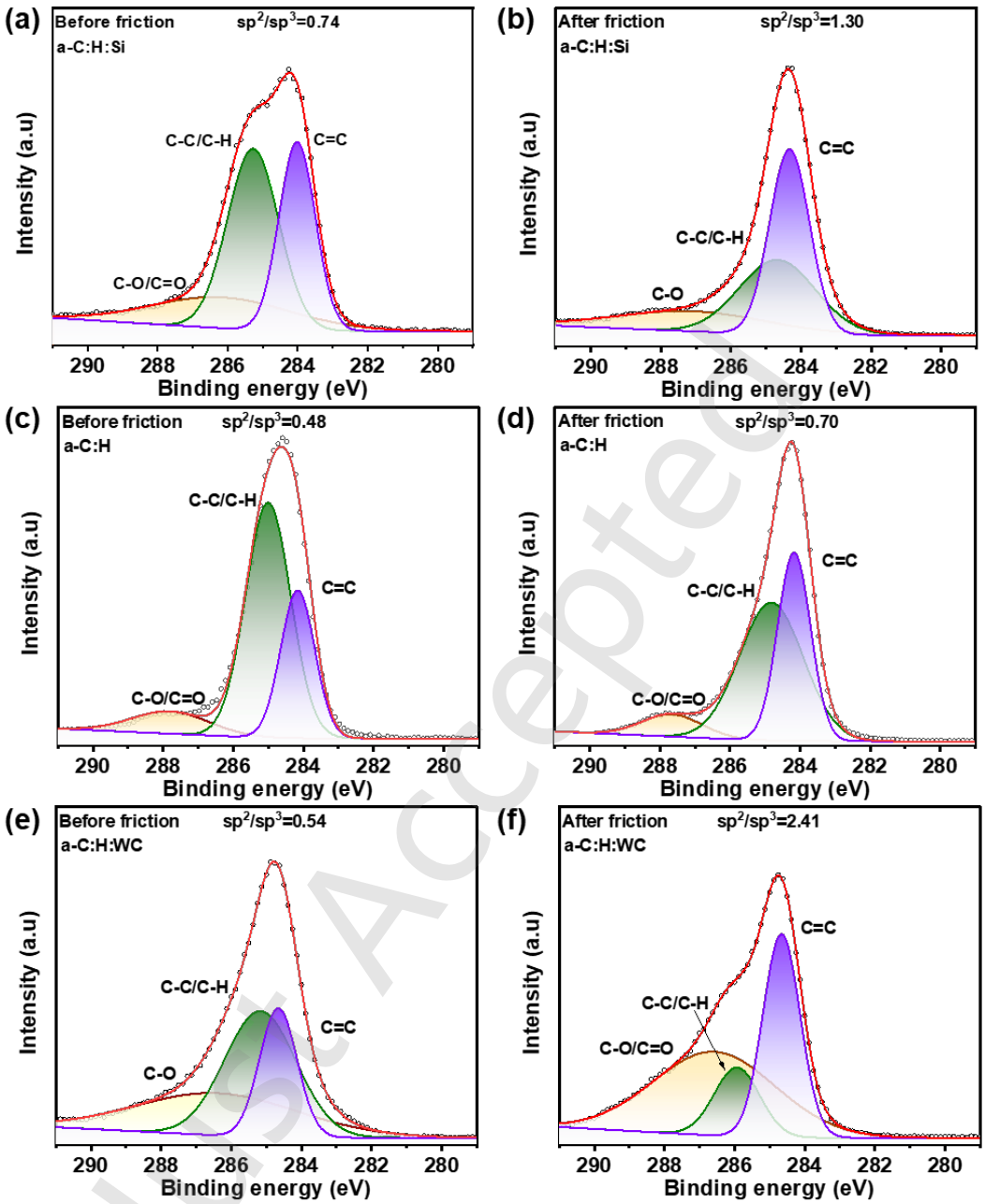

Fig. 4 XPS spectra of C1s on the DLC film surfaes. (a) A-C:H:Si original surface before friction; (b) A-C:H:Si worn track region after friction; (c) A-C:H original surface before friction; (d) A-C:H worn track region after friction; (e) A-C:H:WC original surface before friction; (f) A-C:H:WC worn track region after friction.

3.4.2 Loose-structured water molecules induce low friction coefficient of DLC on ice surface

To clarify the shear behavior of interfacial water molecules during friction under ice conditions, we conducted a thorough investigation using SFG spectroscopy. The SFG experiments were conducted at

room temperature. Therefore, using the molecular structure of water probed at room temperature to explain the friction mechanism on ice surfaces has certain limitations. For low temperature ice surface detection technology of SFG is limited in our laboratory. We measured friction coefficients of the five materials under ambient aqueous conditions. Establishing a relationship between the SFG results and the friction results obtained from AFM measurements at room temperature was scientifically more reasonable. The law of interfacial shear behavior in water environment by AFM was shown in Fig. S2. The experimental results demonstrated that the underwater microscopic friction coefficient of various materials follow the same trend as their macroscopic ice friction coefficient.

The SFG spectroscopy method allowed us to probe hydrogen bonding interactions and the distribution of water molecules at material interfaces. In Fig. 5(a), we illustrate the SFG measurement setup and its underlying principles, while Fig. 5(b) displays the SFG spectra obtained from all five material surfaces. According to previous reports[71], the characteristic peaks at 3400 cm^{-1} and 3200 cm^{-1} correspond to distinct water structures. The 3400 cm^{-1} peak represents "liquid-like" water molecules with disordered structure and relatively weak hydrogen bonds. Arrangement of "liquid-like" water molecules at the interface was shown in Fig. 5(d). The 3200 cm^{-1} peak indicates "ice-like" water molecules with ordered structure and stronger hydrogen bonds. Arrangement of "ice-like" water molecules at the interface was described in Fig. 5(c). The peak intensity ratio ($I_{3400\ cm^{-1}}/I_{3200\ cm^{-1}}$)[72] can be used to analyze the distribution form of water molecules. As shown in Fig. 5(e), this ratio exhibited a strong correlation with ice friction coefficient. Fig. 5(f) shown that materials with $I_{3400\ cm^{-1}}/I_{3200\ cm^{-1}} > 1.2$ consistently demonstrated lower friction coefficient than those with smaller ratio. It could be inferred that the SFG spectrum of the DLC film surface exhibited a relatively high $I_{3400\ cm^{-1}}/I_{3200\ cm^{-1}}$ peak intensity ratio, indicating that the water molecules tend towards "liquid-like" state. The arrangement of water molecules on the material surface was relatively disordered, with weak hydrogen bonds predominating. The interaction forces between water molecules and the interface are relatively weak, resulting in small shear force and a low friction coefficient. On the surfaces of SUJ2

and Si_3N, the SFG spectroscopy shown a lower $I_{3400\ cm^{-1}}/I_{3200\ cm^{-1}}$ peak intensity ratio, indicating that the water molecules tend towards "ice-like" state. At this moment, the arrangement of water molecules on the material surface is notably organized, characterized by robust hydrogen bonds that create a crystal-like structure. The interaction forces between the water molecules and the interface are substantial, resulting in heightened friction.

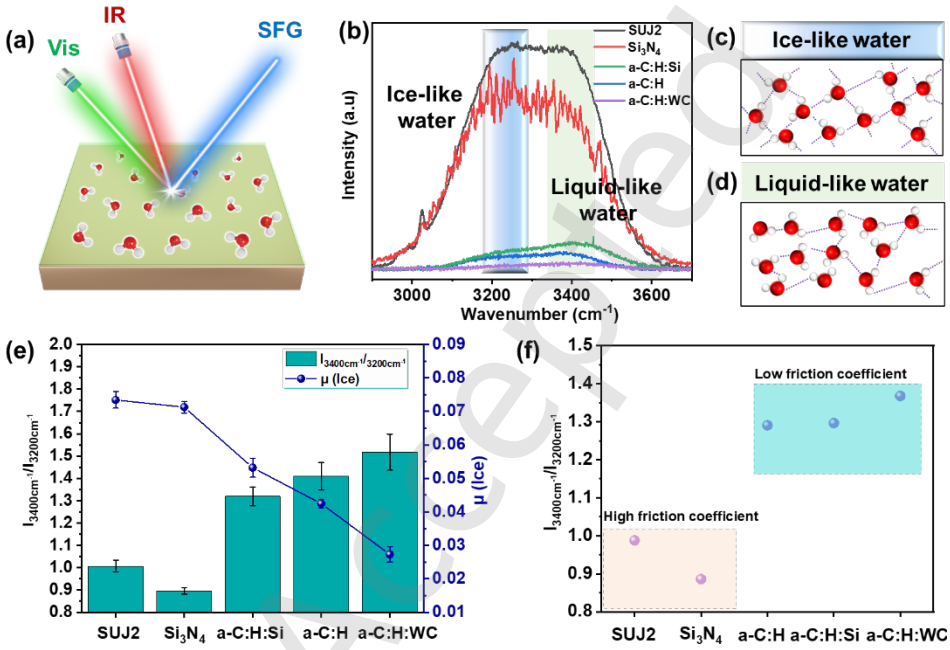

Fig. 5 The SFG spectroscopy of different surfaces. (a) SFG spectroscopy schematic diagram; (b) SFG spectroscopy of the material surface in the 2900-3700 cm^{-1}; (c) Arrangement of "ice-like" water molecules at the interface; (d) Arrangement of "liquid-like" water molecules at the interface; (e) Different materials peak intensity ratio($I_{3400\ cm^{-1}}/I_{3200\ cm^{-1}}$) and ice surface friction coefficient; (f) Relationship diagram between peak intensity ratio and friction coefficient.

3.4.3 Effects of materials to interfacial water structure and shearing behavior via MD simulations

To more intuitively verify the influence of water molecular structure on frictional behavior during ice sliding, molecular dynamics simulations were performed to model ice friction for hydrogenated amorphous carbon (a-C:H) and steel (Fe) sliding against ice. The a-C:H and Fe surfaces closely mimic the chemical composition and structural characteristics of the DLC films and SUJ2 used in our

experiments. The a-C:H/ice system consisted of an a-C:H slab at the top and a fixed ice substrate at the bottom, with the initial model shown in Fig. 7(a). The Fe/ice system comprised a top Fe slab and a fixed bottom ice substrate, as illustrated in Fig. 7(b). In both models, a 40 Å thick water molecules layer was placed between the top and bottom slabs to simulate realistic ice friction conditions. Initially, this water molecules layer adopted the TIP5P-E model of hexagonal ice (Ih), which spontaneously melted or changed arrangement structure as sliding progressed. The top and bottom slabs, along with the intervening water molecules layer, shared identical dimensions in the x and y directions and detailed parameters were provided in Section 2.6. Snapshots from the simulations are presented in Fig. 7(c) and 7(d). In the a-C:H/ice system, a portion of the ice layer adjacent to the fixed bottom ice substrate did not fully melt, whereas in the Fe/ice system, the entire intermediate ice layer melted during sliding. The velocity profiles of water molecules along the Z-direction for both material surfaces were shown in Fig. 7(e). When the a-C:H slider moved, about 25 Å thick water layer adjacent to the fixed ice substrate exhibited nearly zero velocity, whereas the 15 Å thick water layer near the slider moved together with it. In contrast, on the Fe surface, the velocity of water molecules near the slider gradually increased along the Z-direction, exhibiting a velocity gradient resembling Couette flow[46], which consistent with that a film thickness was fully capable of supporting Couette flow once continuity was established[23]. The a-C:H models exhibit plug-like flow (high slip) while Fe models exhibit Couette flow (low slip)[46]. The layering of the water film was analyzed using the hydrogen bond concentration distribution (Fig. 7(f)) and water molecules density distribution (Fig. 7(g)). Each peak in the density profile represented one molecular layer. In the a-C:H system, the water film adjacent to the ice substrate displayed a well-defined, ordered structure resembling that of the fixed ice substrate, explaining the observation in Fig. 7(c) that the ice layer near the substrate did not fully melt. In contrast, in the Fe/ice system, no distinct layering was observed near the ice substrate, indicating more complete melting of the water film during sliding. Notably, the rightmost peaks in the water number density distributions near the slider revealed that the first and second water layers

adjacent to the Fe surface exhibited significantly higher densities than those near the a-C:H surface, implying stronger hydrogen bonding and molecular interactions, which hindered solid-liquid separation and consequently resulted in a higher ice friction coefficient for Fe. Furthermore, the angular distribution of water molecules within the water film was analyzed. Profile of angle ϕ between the normal vector of xy plane and the dipole vector of water molecule of different models along Z axis were presented in Fig. 7(h). Water molecules adjacent to the Fe slider exhibited distinct layering, indicating ordered molecular structure. In contrast, the angular distribution of water molecules near the a-C:H surface remained uniform without significant variation, suggesting a loose and disordered molecular arrangement. These results directly demonstrate the mechanism by which loosely structured water molecules on material surfaces reduce ice friction.

The molecular dynamics simulation results were statistically analyzed, as presented in Fig. 7(i). In this analysis, the solid-liquid interaction energy was defined as the interaction energy between the slider and water molecules ($E_{top\text{-}water}$). The interaction energy between the first-layer water molecules (adjacent to the slider) and the remaining water molecules was denoted as $E_{top\text{-}water\text{-}water}$. The number of hydrogen bonds at the slider surface was represented as N-HB. At the a-C:H/ice interface, both the $E_{top\text{-}water}$ and the $E_{top\text{-}water\text{-}water}$ were relatively weak, and the number of hydrogen bonds at the solid-liquid interface was low. These factors collectively contributed to a lower friction coefficient for the a-C:H/ice system compared to the Fe/ice system. The ice substrate consisted of regular hexagonal ice crystals.

MD results suggest that the most critical factor governing the frictional behavior of ice is the molecular structure of water at the solid-liquid interface. Owing to the lower water molecules density and fewer hydrogen bonds at the a-C:H surface, the water molecules were more loosely arranged and disordered, leading to a weaker solid-liquid interaction energy. This facilitated the detachment of water molecules from the slider surface, thereby reducing frictional forces at the contact interface. In contrast, the Fe surface exhibited higher water molecules density, a greater number of hydrogen bonds, and a more

ordered arrangement of water molecules, resulting in a larger solid-liquid interaction energy with water.

Consequently, the Fe surface displayed a higher ice friction coefficient.

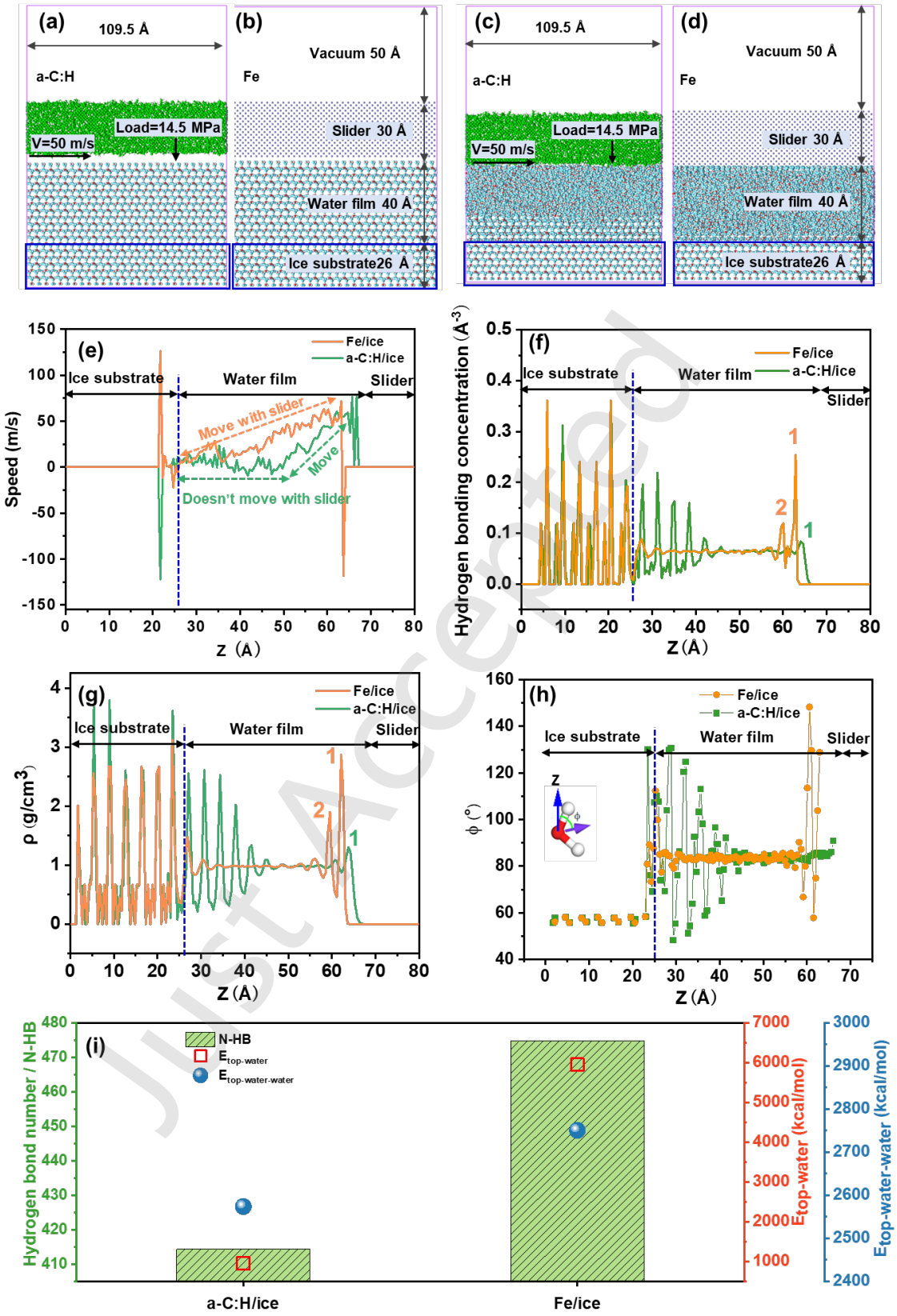

Fig. 6 Molecular dynamics (MD) simulation on the effects of material to interfacial water molecules structure and shearing behavior. (a) Sliding simulation models consisted of a moving slider at the top,

a fixed ice at the bottom, and a sandwiched ice film: (a) a-C:H/ice, (b) Fe/ice. The slider was moving with sliding velocity Vx = 50 m/s in the x direction under normal pressure of 14.5 MPa. The green, gray, red, white, and light blue balls indicate C, Fe, O, H, and TIP5P-E dummy atoms, respectively. A snapshot of sliding simulation: (c) a-C:H/ice, (d) Fe/ice. (e) The velocity (Vx) profile of water molecules of different models along Z-direction. (f) The hydrogen bonding concentration of water molecules of different models along Z-direction. (g) Density profiles of water molecules of different models along Z-direction. (h) Profile of angle ϕ between the normal vector of xy plane and the dipole vector of water molecule of different models along Z axis. (i) The number of hydrogen bonds (N-HB) and the interaction energy between the top slider and the water film ($E_{top\text{-}water}$), as well as the interaction energy between first layer water film on top slider and the rest water ($E_{top\text{-}water\text{-}water}$).

3.5 Mechanism of friction reduction on ice surface

The synergistic effects of surface graphitization and "liquid-like" water molecules were identified as the contributors to DLC film reduction friction: (i) The graphitized area had a very low shear strength due to its low van der Waals forces, so the occurred of graphitization will minimize the friction performance of the material. Surface graphitization was a typical mechanism for explaining DLC friction reduction. However, graphitization occurs under the friction of certain time and pressure. DLC materials showed low friction at the beginning of friction. Consequently, in addition to the graphitization mechanism, there are other synergistic mechanisms that contribute to the reduction of the friction coefficient in the DLC/ice system. (ii) Innovative discovered that DLC films had a higher proportion of "liquid-like" water molecules on their surface, which decreased the friction coefficient. The peak intensity ratio ($I_{3400cm^{-1}}/I_{3200cm^{-1}}$) of DLC films tested by SFG were relatively high than SUJ2 and Si_3N_4. The proportion of water molecules in the "liquid-like" structure was significant, indicating that their arrangement was relatively disordered. The surface of the DLC film exhibited a negative charge, causing the positively charged hydrogen atoms in the water molecules to be adsorbed onto it. As liquid water molecules dominated the interface, each water molecule formed two to three hydrogen

bonds, as illustrated in Fig. 5(d). Consequently, the hydrogen bond lengths were elongated, resulting in weaker hydrogen bonds between the water molecules. This phenomenon contributed to the formation of a weak shear layer at the interface. Additionally, the interaction between the DLC material and the ice surface was minimal, leading to reduced shear forces from the water molecules during interfacial sliding and ultimately resulting in a low coefficient of friction. In addition, the friction coefficient and the peak intensity ratio ($I_{3400cm}^{-1}/I_{3200cm}^{-1}$) of a-C:H:Si, a-C:H, and a-C:H:WC on ice surface showed a progressive decrease. Therefore, loose interfacial water molecule induced low friction on ice was the main factor in reducing friction.

Nevertheless, the peak intensity ratio ($I_{3400cm}^{-1}/I_{3200cm}^{-1}$) of SUJ2 and Si_3N_4 surfaces were relatively smaller, and the proportion of "ice-like" water molecules structure was large. At this point, the configuration of water molecules was relatively organized, with each molecule forming four hydrogen bonds (Fig. 5(c)). The shorter length of these hydrogen bonds contributed to their strength, leading to a more regular square arrangement of the water molecules. Due to the strong interactions between the SUJ2 or Si_3N_4 and the ice surface during sliding, the water molecules underwent increased shear stresses, resulting in a higher friction coefficient. The friction mechanisms for various materials on ice are shown in Fig. 7.

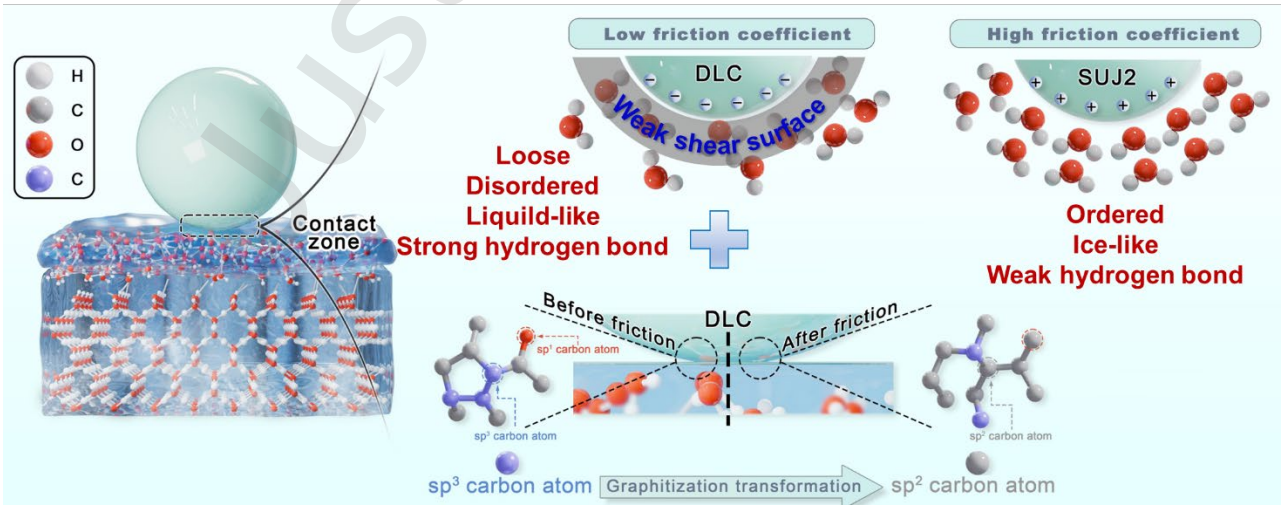

Fig. 7 Mechanism diagram of different materials on ice

4 Conclusions

The study investigated three categories of materials: bearing steel (commonly used on ice/in water friction scenarios), silicon nitride (excellent water-lubrication properties), ceramic material (SiO_2 and TiO_2) and three hydrogenated DLC films (a-C:H:Si, a-C:H, a-C:H:WC). Through a series of macroscopic ice friction and microscopic underwater friction experiments, the tribological behaviors of these materials were systematically characterized. XPS, Raman spectroscopy, MD simulation and SFG spectroscopy were employed to investigate chemical bonding and the molecular structures of interfacial water. This approach facilitated a comprehensive exploration, from the overarching macroscopic friction laws to microscopic interfacial molecular structures. The main research conclusions are as follows:

(1) DLC films demonstrated superior friction performance compared to SUJ2 and Si_3N_4 under different working conditions in ice friction (sliding speed, load, temperature). When the friction speed on the ice surface was 1.55 m/s, the temperature was -7 ℃, and the load was 9 N, the friction coefficients of a-C:H:Si, a-C:H, and a-C:H:WC films on the ice surface were reduced by 21.5%, 38.7%, and 58.6%, respectively compared to SUJ2.

(2) The wear on the ice surface of SUJ2 and DLC films was predominantly due to abrasive wear, with the wear area of the DLC film being significantly smaller than that of SUJ2. Additionally, the a-C:H film exhibited signs of fatigue wear. Although Si_3N_4, due to its higher hardness showed no significant wear.

(3) The friction process increased the ratio of sp^2/sp^3 on the surface of DLC material. Due to the large load of local contact at the shear interface, friction induced the C-H bond in sp^3 hybrid bonds to break. The removal of H would induce the transformation of the sp^3 hybrid bonds into sp^2 hybrid bond structures, resulting in graphitization and favorable lower friction coefficient on the ice surface.

(4) The distribution of water molecules showed that the peak intensity ratio of $3400cm^{-1}$ to $3200cm^{-1}$ on the DLC material surface was relatively large, suggesting that the water molecules on the DLC

material surface was relatively disordered and tended towards a “liquid-like” structure. The interaction between the DLC material and the ice surface was weak, shear force between the material and water molecules decreased, resulting in a lower friction coefficient on the ice surface. This was the dominant mechanism for the low friction of the ice surface.

(5) Molecular dynamics simulations unambiguously confirmed that, during ice friction against hydrogenated amorphous carbon, the interfacial water molecules adopt a more loosely packed and disordered arrangement, accompanied by a reduced number of hydrogen bonds at the interface, lower water density, and weaker interaction energy.

This work achieved key advancement was DLC exhibits an exceptionally low friction coefficient on ice surfaces. Building on the traditional graphitization friction reduction mechanism of DLC, a novel perspective had emerged that loosely structured interfacial water molecules or a higher proportion of high activity water molecules at the solid-liquid interface facilitates for reducing ice friction. The ice surface low friction mechanism is to some extent consistent with the observations reported by Baran[46] and Liefferin[24]. Our results offer complementary molecular level insights into this mechanism, particularly through the combined use of nonlinear spectroscopy and MD simulations. The arrangement of water molecules on material surfaces results from a combination of their physical and chemical properties. This insight could lead to a unified approach for assessing friction performance across various materials with different types and properties, paving the way for innovative research and development in low friction technologies for icy even water environments.

Declaration of competing interest

The authors have no competing interests to declare that are relevant to the content of this article.

Acknowledgements

This work was financially supported by the support of the NSFC Excellence Research Group (No.52488101), Fundamental and Interdisciplinary Disciplines Breakthrough Plan of the Ministry of Education of China(No. JYB2025XDXM209) and the National Key Research and Development Program of China (Grant No. 2020YFF0304600).

Electronic Supplementary Material (ESM)

Supplementary data to this article can be found at Supporting Information.

References

[1] Dong C, Meng YN, Liu Y, Huang ZT, Ma LR. Study on the ice friction characteristics. *Cold Regions Science and Technology* **216**: 104010 (2023).

[2] Canale L, Comtet J, Niguès A, Cohen C, Clanet C, Siria A, et al. Nanorheology of Interfacial Water during Ice Gliding. *Physical Review X* **9**(4): 041025 (2019).

[3] Kietzig A-M, Hatzikiriakos SG, Englezos P. Ice friction: The effects of surface roughness, structure, and hydrophobicity. *Journal of Applied Physics* **106**(2): 024303 (2009).

[4] Hu J, Zhou L. Experimental and numerical study on ice resistance for icebreaking vessels. *International Journal of Naval Architecture and Ocean Engineering* **7**(3): 626-639 (2015).

[5] Petrenko VF. The effect of static electric fields on ice friction. *Journal of Applied Physics* **76**(2): 1216-1219 (1994).

[6] Kietzig A-M, Hatzikiriakos SG, Englezos P. Physics of ice friction. *Journal of Applied Physics* **107**(8): 081101 (2010).

[7] Li J, Chen HS, Stone HA. Ice lubrication for moving heavy stones to the Forbidden City in 15th- and 16th-century China. *Proceedings of the National Academy of Sciences* **110**(50): 20023-20027 (2013).

[8] Rosenberg R. Why Is Ice Slippery? *Physics Today* **58**(12): 50-54 (2005).

[9] Bowden FP, Hughes TP. The Mechanism of Sliding on Ice and Snow. *Proceedings of the Royal Society of London Series A, Mathematical and Physical Sciences* **172**(949): 280-298 (1939).

[10] Zhang X, Huang YL, Ma ZS, Niu LY, Sun CQ. From ice superlubricity to quantum friction: Electronic repulsivity and phononic elasticity. *Friction* **3**(4): 294-319 (2015).

[11] Gurney C. Surface Forces in Liquids and Solids. *Proceedings of the Physical Society Section A* **62**(10): 639 (1949).

[12] Conde MM, Vega C, Patrykiejew A. The thickness of a liquid layer on the free surface of ice as obtained from computer simulation. *The Journal of chemical physics* **129**(1): 014702 (2008).

[13] Llombart P, Noya EG, MacDowell LG. Surface phase transitions and crystal habits of ice in the atmosphere. *Science Advances* **6**(21): eaay9322 (2020).

[14] Orem MW, Adamson AW. Physical adsorption of vapor on ice: II. n-alkanes. *Journal of Colloid and Interface Science* **31**(2): 278-286 (1969).

[15] Kvlividze VI, Kiselev VF, Kurzaev AB, Ushakova LA. The mobile water phase on ice surfaces. *Surface Science* **44**(1): 60-68 (1974).

[16] Strausky H, Krenn JR, Leitner A, Aussenegg FR. Sliding plastics on ice: fluorescence spectroscopic studies on interfacial water layers in the μm thickness regime. *Applied Physics B* **66**(5): 599-602 (1998).

[17] Ikeda Fukazawa T, Kawamura K. Molecular-dynamics studies of surface of ice Ih. *The Journal of Chemical Physics* **120**(3): 1395-1401 (2004).

[18] Li Y, Somorjai GA. Surface Premelting of Ice. *The Journal of Physical Chemistry C* **111**(27): 9631-9637 (2007).

[19] Döppenschmidt A, Butt HJ. Measuring the Thickness of the Liquid-like Layer on Ice Surfaces with Atomic Force Microscopy. *Langmuir* **16**(16): 6709-6714 (2000).

[20] Hong JN, Tian Y, Liang TC, Liu XM, Song YZ, Guan D, et al. Imaging surface structure and premelting of ice Ih with atomic resolution. *Nature* **630**(8016): 375-380 (2024).

[21] Lever JH, Asenath-Smith E, Taylor S, Lines AP. Assessing the Mechanisms Thought to Govern Ice and Snow Friction and Their Interplay With Substrate Brittle Behavior. *Frontiers in Mechanical Engineering* **7**: 690424 (2021).

[22] Tusima K. Adhesion Theory for Low Friction on Ice. In: New Tribological Ways. Ghrib TH, Ed. London: IntechOpen, 2011: 301-328.

[23] Weber B, Nagata Y, Ketzetzi S, Tang F, Smit WJ, Bakker HJ, et al. Molecular Insight into the Slipperiness of Ice. *The Journal of Physical Chemistry Letters* **9**(11): 2838-2842 (2018).

[24] Liefferink RW, Hsia F-C, Weber B, Bonn D. Friction on Ice: How Temperature, Pressure, and Speed Control the Slipperiness of Ice. *PHYSICAL REVIEW X* **11**(1): (2021).

[25] Demmenie M, Kolpakov P, Nagata Y, Woutersen S, Bonn D. Scratch-Healing Behavior of Ice by Local Sublimation and Condensation. *The Journal of Physical Chemistry C* **126**(4): 2179-2183 (2022).

[26] Demmenie M, Reus L, Kolpakov P, Woutersen S, Bonn D, Shahidzadeh N. Growth and Form of Rippled Icicles. *Physical Review Applied* **19**(2): 024005 (2023).

[27] Demmenie M, Gorin B, Kolpakov P, Smith S, Kellay H, Bonn D. Partial wetting of water on ice. *Physical Review Fluids* **10**(5): 054002 (2025).

[28] Nagata Y, Hama T, Backus EHG, Mezger M, Bonn D, Bonn M, et al. The Surface of Ice under Equilibrium and Nonequilibrium Conditions. *Accounts of Chemical Research* **52**(4): 1006-1015 (2019).

[29] Hua DY. Friction/Traction Behavior of EHL. In: Encyclopedia of Tribology. Wang QJ, Chung Y-W, Ed. Boston: Springer, 2013: 1398-1404.

[30] Jansons E, Lungevics J, Velkavrh I, Wright T. Ice friction: A brief review of the influencing factors and experimental methods. *Friction* **13**(9): 9441076 (2025).

[31] Scherge M, Böttcher R, Spagni A, Marchetto D. High-Speed Measurements of Steel–Ice Friction: Experiment vs. Calculation. *Lubricants* **6**(1): 26-26 (2018).

[32] Maeno N, Arakawa M, Yasutome A, Mizukami N, Kanazawa S. Ice-ice friction measurements, and water lubrication and adhesion-shear mechanisms. *Canadian Journal of Physics* **81**(1): 241-249 (2003).

[33] Schulson EM. Friction of sea ice. *Philosophical Transactions of the Royal Society A: Mathematical, Physical and Engineering Sciences* **376**(2129): 20170336 (2018).

[34] Dong C, Liu Y, Han TY, Zhou X, Meng YN, Tian Y, et al. Effect of hydrated ions and wettability on ice friction. *Friction* **13**(7): 9440972 (2025).

[35] Kietzig A-M, Hatzikiriakos SG, Englezos P. Ice friction: the effect of thermal conductivity. *Journal of Glaciology* **56**(197): 473-479 (2010).

[36] Dong C, Liu Y, Meng YN, Du SN, Zhu SC, Tian Y, et al. Ion-specific ice provides a facile approach for reducing ice friction. *Journal of Colloid and Interface Science* **675**: 451-460 (2024).

[37] Okazaki Y, Azuma S, Fukuhara D, Katayama I, Sekine Y, Saruya T. Low-temperature friction experiments on ice–salt mixtures: Implications for the strength of ice plate boundaries on Europa. *Icarus* **411**: 115961 (2024).

[38] Xie ZL, Jiao J, Yang K, Zhang H. A state-of-art review on the water-lubricated bearing. *Tribology International* **180**: 108276 (2023).

[39] Deng MM, Li JJ, Zhang CH, Ren J, Zhou NN, Luo JB. Investigation of running-in process in water-based lubrication aimed at achieving super-low friction. *Tribology International* **102**: 257-264 (2016).

[40] Ma LR, Gaisinskaya-Kipnis A, Kampf N, Klein J. Origins of hydration lubrication. *Nature Communications* **6**(1): 6060 (2015).

[41] Luo JB, Liu M, Ma LR. Origin of friction and the new frictionless technology—Superlubricity: Advancements and future outlook. *Nano Energy* **86**: 106092 (2021).

[42] Erdemir A, Fontaine J, Donnet C. *Tribology of Diamond-Like Carbon Films*. New York: Springer Science, 2008.

[43] Liu QJ, Zhang NC, Liu FS, Liu ZT. Structural, elastic, electronic and optical properties of various mineral phases of TiO2 from first-principles calculations. *Physica Scripta* **89**(7): 075703 (2014).

[44] Dai CL, Chang YM. A resonant method for determining mechanical properties of Si3N4 and SiO2 thin films. *Materials Letters* **61**(14): 3089-3092 (2007).

[45] Han TY, Zhang CH, Chen XC, Li JJ, Wang WQ, Luo JB. Contribution of a Tribo-Induced Silica Layer to Macroscale Superlubricity of Hydrated Ions. *The Journal of Physical Chemistry C* **123**(33): 20270-20277 (2019).

[46] Baran Ł, Llombart P, Rżysko W, MacDowell LG. Ice friction at the nanoscale. *Proceedings of the National Academy of Sciences* **119**(49): e2209545119 (2022).

[47] Wang XZ, Liu Y, Ma LR, Xu XF, Tian Y. Reclined trend of alkyl chain of sodium dodecylbenzenesulfonate molecules induced by friction. *Friction* **10**(9): 1353-1364 (2022).

[48] Chenoweth K, van Duin ACT, Goddard WA. ReaxFF Reactive Force Field for Molecular Dynamics Simulations of Hydrocarbon Oxidation. *The Journal of Physical Chemistry A* **112**(5): 1040-1053 (2008).

[49] Dauber-Osguthorpe P, Roberts VA, Osguthorpe DJ, Wolff J, Genest M, Hagler AT. Structure and energetics of ligand binding to proteins: Escherichia coli dihydrofolate reductase-trimethoprim, a drug-receptor system. *Proteins: Structure, Function, and Bioinformatics* **4**(1): 31-47 (1988).

[50] Rick SW. A reoptimization of the five-site water potential (TIP5P) for use with Ewald sums. *The Journal of Chemical Physics* **120**(13): 6085-6093 (2004).

[51] García Fernández R, Abascal JLF, Vega C. The melting point of ice Ih for common water models calculated from direct coexistence of the solid-liquid interface. *The Journal of Chemical Physics* **124**(14): 144506 (2006).

[52] Wei XP, Xiao HP, Ni J. Studies of ice melting using molecular dynamics. *Molecular Simulation* **36**(11): 823-830 (2010).

[53] Plimpton S. Fast Parallel Algorithms for Short-Range Molecular Dynamics. *Journal of Computational Physics* **117**(1): 1-19 (1995).

[54] Nose S. Constant Temperature Molecular Dynamics Methods. *Progress of Theoretical Physics Supplement* **103**: 1-46 (1991).

[55] Hockney RW, Eastwood JW. *Computer Simulation Using Particles*. New York: CRC Press, 1988.

[56] Schulson EM. Low-speed friction and brittle compressive failure of ice: fundamental processes in ice mechanics. *International Materials Reviews* **60**(8): 451-478 (2015).

[57] Persson BNJ. Ice friction: Role of non-uniform frictional heating and ice premelting. *The Journal of Chemical Physics* **143**(22): 224701 (2015).

[58] Blackford JR. Sintering and microstructure of ice: a review. *Journal of Physics D: Applied Physics* **40**(21): R355 (2007).

[59] Lozowski E, Szilder K, Maw S. A model of ice friction for a speed skate blade. *Sports Engineering* **16**(4): 239-253 (2013).

[60] Colbeck SC. The Kinetic Friction of Snow. *Journal of Glaciology* **34**(116): 78-86 (1988).

[61] Du F. Analytical Theory of Ice-Skating Friction with Flat Contact. *Tribology Letters* **71**(1): 5 (2022).

[62] Tóth S, Veres M, Füle M, Koós M. Influence of layer thickness on the photoluminescence and Raman scattering of a-C:H prepared from benzene. *Diamond and Related Materials* **15**(4): 967-971 (2006).

[63] Ferrari AC, Robertson J. Interpretation of Raman spectra of disordered and amorphous carbon. *Physical Review B* **61**(20): 14095-14107 (2000).

[64] Zhang CX, Deng WL, Xu JX, Yu QY, Wang YH, Tian JS, et al. Effect of a-C:H:Si interlayers on the mechanical and superlubricious properties of hydrogenated amorphous carbon films. *Thin Solid Films* **753**: 139275 (2022).

[65] Liu YH, Wang L, Liu T, Zhang P. Effect of normal loads and mating pairs on the tribological properties of diamond-like carbon film. *Wear* **486-487**: 204083 (2021).

[66] Liu Y, Meletis EI. Evidence of graphitization of diamond-like carbon films during sliding wear. *Journal of Materials Science* **32**(13): 3491-3495 (1997).

[67] Liu Y, Erdemir A, Meletis EI. An investigation of the relationship between graphitization and frictional behavior of DLC coatings. *Surface and Coatings Technology* **86-87**: 564-568 (1996).

[68] Tian J, Chen X, Xu J, Yu J, Yu Q, Zhang C, et al. Operando formation of multiphase heterostructure for achieving macroscale superlubricity with ultra-long lifetime under high contact stress. *Materials Today Chemistry* **28**: 101363 (2023).

[69] Erdemir A, Donnet C. Tribology of diamond-like carbon films: recent progress and future prospects. *Jphysd Applphys* **39**(18): R311 (2006).

[70] Jang S, Chen Z, Kim SH. Origin of superlubricity of diamond-like carbon (DLC). *Friction* **13**(1): 9440995 (2025).

[71] Scatena LF, Brown MG, Richmond GL. Water at Hydrophobic Surfaces: Weak Hydrogen Bonding and Strong Orientation Effects. *Science* **292**(5518): 908-912 (2001).

[72] Ma PS, Liu Y, Han K, Tian Y, Ma LR. Hydration lubrication modulated by water structure at TiO2-aqueous interfaces. *Friction* **12**(4): 591-605 (2023).

Yuan Liu received her Ph.D. degree from Tsinghua University in 2024. She is currently worked as a postdoctoral research fellow working with Prof. Jianbin LUO and Prof. Liran MA at the State Key Laboratory of Tribology in Advanced Equipment, Tsinghua University, Beijing, China. Her major

research interests are mainly about orientation and structure of interface molecular, lubrication, drag reduction technology, and sum frequency generation spectroscopy.

Liran Ma received her Ph.D. degree in 2010 from Tsinghua University, China. Following a postdoctoral period at Weizmann Institute of Science, Israel, she is now working as an associate professor in State Key Laboratory of Tribology in Advanced Equipment, Tsinghua University, China. She has long been engaged in basic theoretical and technological innovation research on film lubrication and superlubricity. She has published over 100 SCI papers with more than 2,000 citations. She won the Maple Leaf Young Scholar Award, the Youth Project of National High-level Talent Support Program, the Science and Technology Progress Award of China Machinery Industry Science and Technology Award, Advanced person of Tsinghua University and was supported by the Excellent Youth Program of National Natural Science Foundation of China.